Int. J. Electrochem. Sci., 14 **(2019)** 161 – 172, doi: 10.20964/2019.01.29

International Journal of
ELECTROCHEMICAL
SCIENCE
www.electrochemsci.org

Effect of Temperature on Corrosion Behavior of X65 Steel in Simulated Deep Sea Environment

Liqin Wang, Zhiming Gao, Yingjie Liu, Xibo Lu, Can Wang, Wenbin Hu*

School of Material Science and Technology, Tianjin University, Tianjin, 30072, China
Engineering Research Center of Composite and Functional Materials,Ministry of Education, Tianjin, 30350, China
*E-mail: gaozhiming@tju.edu.cn

Received: 9 September 2018 / *Accepted:* 16 October 2018 / *Published:* 30 November 2018

The influence of temperature on the corrosion behavior of X65 steel under simulated abyssal conditions have been investigated using electrochemical methods, Raman spectroscopy and 3D microscopy. EIS results indicated that the R_{ct} (charge transfer resistance) decreased gradually and the film density of the corrosion layer decreased with increasing temperatures. Polarization curves indicated that the corrosion current densities increased and the self-corrosion potentials shifted negatively with increasing temperatures. The corrosion morphology manifested that the dense corrosion product films were formed at lower temperatures with pitting corrosion occurring, whilst the corrosion product films had cracks at higher temperatures and the corrosion of X65 steel featured uniform corrosion. The results of Raman spectroscopy showed that the corrosion products were comprised of γ-FeOOH and Fe_3O_4 at 5°C, while they contained γ-FeOOH and α-FeOOH at 25°C. Therefore, the corrosion resistance properties of X65 pipeline steel in abyssal environments decreased as temperature increased.

Keywords: X65 pipeline steel, deep sea environments, temperature, hydrostatic pressure.

1. INTRODUCTION

The deep-sea environment is a very complicated and demanding environment. High hydrostatic pressure, low temperature, salinity, dissolved oxygen and a range of pH levels exist in deep-sea environments [1-2], which means that steel materials often display greater resistance to corrosion in deep-sea environments, when compared to corrosion on land or in shallow seas. The effect of temperature on the corrosion of deep-sea materials is second only to that of dissolved oxygen, which is one of the important factors influencing the corrosion of deep-sea environments [3]. Several literatures on simulating corrosion in abyssal environment mostly focused on the influence of hydrostatic pressure on the corrosion process. For example, Yang [4,8] have reported the stress corrosion cracking of X70 steel was affected by hydrostatic pressure in deep sea environment. Yang [5-7] have reported the effect of hydrostatic pressures on corrosion performance of alloy. However, the influence of temperature is primarily concentrated on investigating corrosion processes in seawater environments at atmospheric pressure [9-17]. Melchers [13] stated that the pitting corrosion rates were almost doubled when the temperature was increased by 10℃ and the corrosion rate increased with the rise in seawater temperature, with other studies [9,17] reporting that increased corrosion rates were linearly correlated to seawater temperature. Yuan [11] supported that the anodic reaction was mainly affected by temperature about corrosion of the steel. However, there is still insufficient knowledge of the mechanism of steel corrosion at low temperatures in high pressure deep-sea environments. The purpose of this study was to examine the low temperature corrosion behavior of X65 pipeline steel in deep sea environments at depths of 1500m, with the aim of determining the mechanism of their corrosion processes under these conditions.

2. EXPERIMENTAL

2.1 Materials

The experimental material is a commercial X65 pipeline steel. The chemical constituent is shown in Table 1.

Table 1. Chemical constituent of X65 pipeline steel for experiments (wt-%)

C	Mn	Si	Cr	P	S	Ni	Ti	V	Nb	Fe
0.05	1.32	0.26	0.023	0.011	0.009	0.026	0.018	0.036	0.029	balance

The microstructure of the X65 pipeline steels is shown in Fig.1, which is composed of polygonal ferrite and granular pearlite.

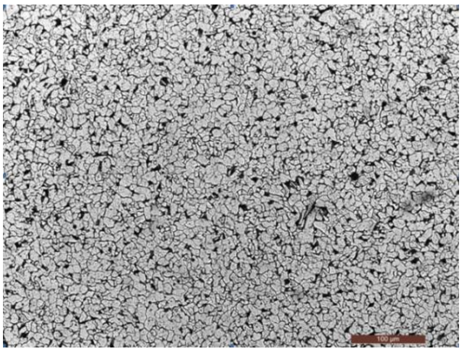

Figure 1. Microstructure of X65 pipeline steel for experiments

2.2 Sample Preparation

The test specimens were machined into tablet specimens with a size of 10 mm×10 mm×1 mm and encapsulated in PVC tubes with epoxy resin. The specimens welded the wires and exposed the area 1 cm^2 to the working face. All the specimens used in this study were successively polished with 2000 grit emery paper and then rinsed with distilled water and anhydrous ethanol. Schematic diagram of high pressure device was shown in Fig.2. All the experiments conditions were as follow: hydrostatic pressure was 15 MPa and pH was 7. The experiment solution was 3.5% NaCl to simulate the seawater.

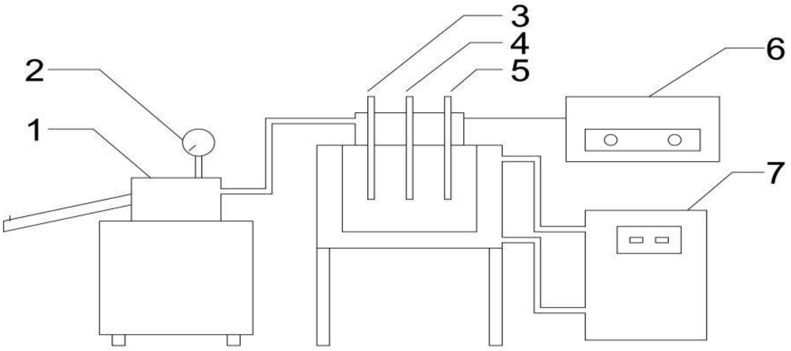

Figure 2. Schematic diagram of high pressure device (1,manual hydraulic press 2, pressure gauge 3, working electrode 4, reference electrode 5, counter electrode 6, control platform 7, low temperature thermostat)

2.3 Electrochemical measurements

The electrochemical measurements were conducted by PARSTA2273. The working electrode, auxiliary electrode (Pt) and reference electrode (Ag/AgCl) constituted three electrodes. Before each test, the open-circuit potentials were conducted for 1800s until the system tended to be stable. The potentiodynamic polarization measurements of X65 carbon steel were conducted from 0.8 V below the open-circuit potentials to 0.4 V at 0.5 mV/s.

The electrochemical impedance spectroscopy (EIS) measurements were measured at a amplitude of the AC signal of 10 mV. The test frequencies ranged from 100 KHZ to 10 mHz.

The electrochemical noise measurements (EN) were conducted by ZF100 equipped with EN module. Each set of EN records recorded with a interval of 0.5 s, which contained 129600 data points.

2.4 Raman spectra

The X65 steel immersed simulated seawater (3.5% NaCl solution) at different temperatures for 48 h. The corrosion products had been examined by using Raman spectrometer (Renishaw 2000) with the 532 nm wavelength laser lines.

2.5 Corrosion morphology

The corrosion morphology of X65 steel after immersing in simulated seawater at 5℃ and 25℃ for 48 h was examined using 3D microscope VHX-2000.

3. RESULTS AND DISCUSSION

3.1 Polarization Curve Measurements

Polarization curves of X65 steel at 15MPa hydrostatic pressure for different temperatures were shown in Fig.3, with their corresponding polarization curve parameters listed in Table 2. These anodic polarization curves revealed active corrosion characteristics at different temperatures, with limited diffusion current densities increasing and corrosion potentials shifting negatively as the temperature increased. From Fig.3, it could be noticed the cathodic process was nearly unchanged from 5°C to 35°C, but the anodic current density increased with increasing temperatures in the same potential. It could be concluded that corrosion was primarily controlled by anodic dissolution. The increase of temperature from 5°C to 35°C can promotes the corrosion reaction kinetics and accelerates the anodic dissolution of metal [18]. However, the cathodic process changed greatly at -5°C, which may be that low temperature decreased diffusion of oxygen and thickness of the stagnant layer. It indicated that corrosion process at -5°C was primarily controlled through cathodic process.

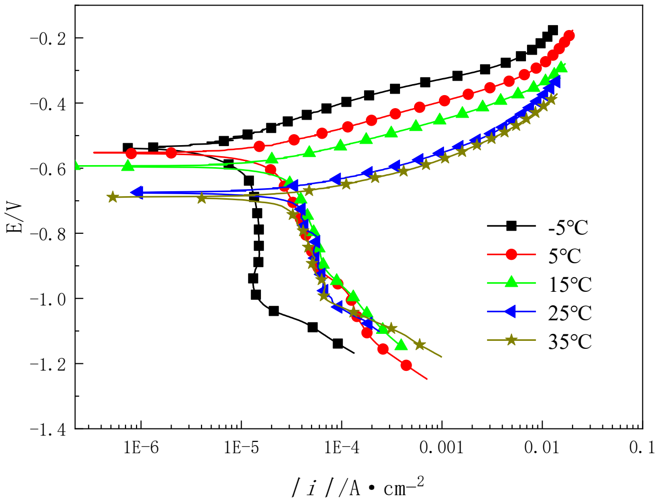

Figure 3. Potentiodynamic polarization curves of X65 steel at different temperatures under 15 MPa (the black curve is -5℃, the red curve is 5°C, the green curve is 15°C, the blue curve is 25°C, the army green curve is 35°C)

Table 2. The related parameters of polarization curve under different temperatures after fitting

Temperature(°C)	E_{corr} (V)	I_{corr} (A·cm^{-2})	b_a (V/dec)
-5	-0.536	9.4×10^{-6}	0.106
5	-0.553	1.6×10^{-5}	0.082
15	-0.594	2.8×10^{-5}	0.088
25	-0.674	3.6×10^{-5}	0.106
35	-0.689	3.7×10^{-5}	0.126

3.2 Electrochemical Impedance Spectroscopy Measurements

The EIS measurements were conducted at various temperatures (-5, 5 , 15, 25 and 35°C) in 3.5% NaCl solution and the results were shown in Fig.4. The module value of impedance decreased from 4600 Ω•cm^2 to 500 Ω•cm^2 with temperature rising from -5°C to 25°C which indicated that the corrosion resistance of X65 decreased with increasing temperatures. It could be seen from the phase angle diagram that the corrosion product films produced at lower temperatures were denser than those formed at higher temperatures [19].

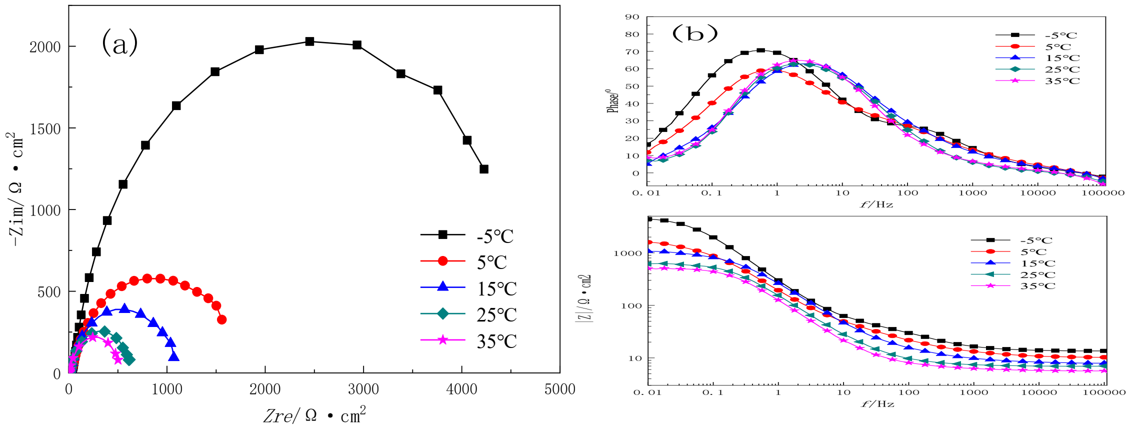

Figure 4. (a) Nyquist plot and (b) Bode plot of X65 steel at different temperatures.(the black curve is -5℃, the red curve is 5°C, the blue curve is 15°C, the cyan curve is 25°C, the pink curve is 35°C)

Interfacial process was simulated using the equivalent circuit shown in Fig.5, with R$_s$ representing the solution resistance, Q$_f$ and R$_f$ corresponding to the adsorption capacitance and the resistance of corrosion products, respectively. Q$_{dl}$ was equivalent to the double layer capacitance, R$_{ct}$ was the charge transfer resistance. Fitted results were listed in Table 3. With rising of the temperature, the solution resistance R$_s$ decreased gradually because the ion activity increased. Moreover, the charge transfer resistance (R$_{ct}$) of X65 steel was measured as 527 Ω·cm^2 at 35°C, with a significantly higher value of 5054 Ω•cm^2 being observed at -5°C. The resistance of the corrosion products (R$_f$) decreased with the increase of temperature, indicating that more defects presented in the corrosion product films on the metal surface, which made it easier for the carrier in the film and the external media to diffuse and for the corrosive medium to access the surface of the metal matrix.

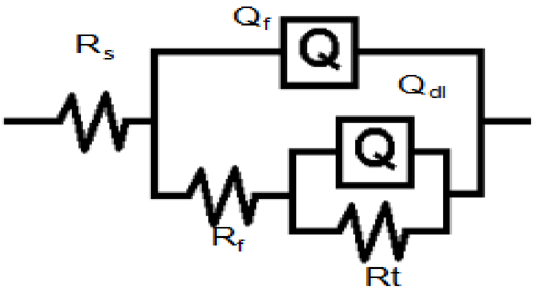

Figure 5. The fitting circuit of Electrochemical Impedance Spectroscopy

Table 3. The related parameters of X65 steel at different temperatures after fitting

Temperature (°C)	R_s ($\Omega\cdot cm^2$)	Q_f ($\mu F\cdot cm^{-2}$)	R_f ($\Omega\cdot cm^2$)	Q_{dl} ($\mu F\cdot cm^{-2}$)	R_{ct} ($\Omega\cdot cm^2$)
-5	13.8	247.5	44.7	430.5	5054
5	10.8	511.1	34.8	530.5	1634
15	8.1	543.8	16.6	293.4	1087
25	7.1	794.1	17.6	499.1	626
35	5.8	572.3	4.1	986.1	527

The Arrhenius formula could be used to calculate the activation energy of the corrosion process:

$$\mathrm{Log}(i_{corr})=\mathrm{Log}(A)-\frac{E_a}{2.303RT} \qquad (1)$$

$$\mathrm{Log}\left(\frac{1}{R_{ct}}\right)=\mathrm{Log}(A)-\frac{E_a}{2.303RT} \qquad (2)$$

where R (8.314 $J\cdot(mol\cdot K)^{-1}$) represents the molar gas constant, T (K) represents the thermodynamic temperature of sea water, E_a ($J\cdot mol^{-1}$) represents the activation energy of the corrosion reaction, A is the Arrhenius constant. The dependence of i_{corr}(a) and R_{ct}(b) on the temperature according to the Arrhenius plot is shown in Fig.6. The Fig.6 shows that the relationship between corrosion rate and temperature change satisfies the Arrhenius formula. The $\mathrm{Log}(i_{corr})-\frac{1}{T}$ plot and $\mathrm{Log}(\frac{1}{R_{ct}})-\frac{1}{T}$ plot are used to calculate the activation energy of corrosion reactions, which are 38.25 $kJ\cdot mol^{-1}$ and 38.07 $kJ\cdot mol^{-1}$, respectively.

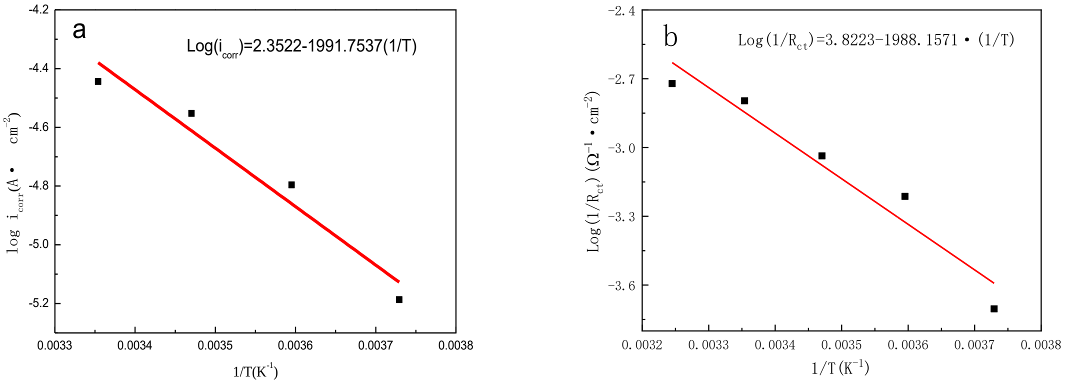

Figure 6. Dependence of i_{corr}(a) and R_{ct}(b) on the temperature according to the Arrhenius plot

3.3 Electrochemical noise

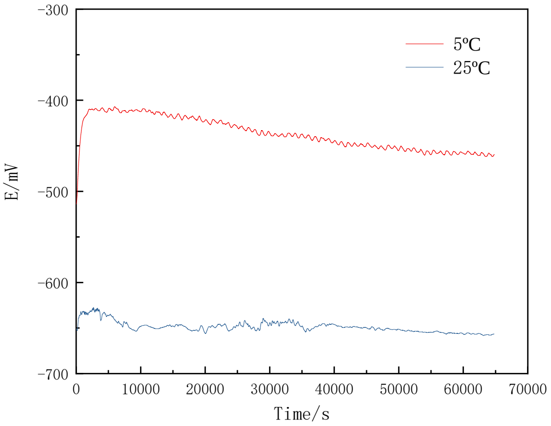

Figure 7. The electrochemical noise of X65 steel during immersion time for 18h at 5°C and 25°C

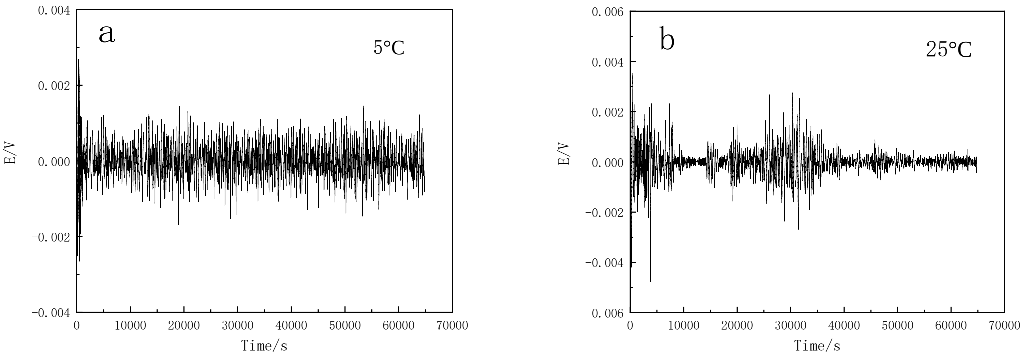

Figure 8. The EN of X65 steel during immersion time for 18h at (a)5°C(b)25°C after direct current trend removal

The potential noise of steel specimens at different temperatures during soaking for 18h was presented in Fig.7. The Fig.8 presented the corresponding noise data after direct current drift removal. The DC drift was removed from the original data using a wavelet analysis method. It was observed that the potential noise fluctuated uniformly with amplitudes of 1 mV under 5°C, while noise levels fluctuations were much more significant at 25°C..

The power spectrum densities (PSD) of X65 steel for different immersion times at (a) 5°C (b)25°C were presented in Fig.9, which were obtained through Fast Fourier Transformation (FFT) of noise data. The PSD parameters, especially the roll-off slope (n), were found to be directly related to the corrosion process and its mechanisms of action [21]. Uruchurtu and Dawson [20] have reported that the PSD plots can be used to characterize the type of attack and provide a means to detect the presence of pitting corrosion. The more than -20 db/decade are indicative of pitting corrosion, whereas a roll off slope of shallow slopes of -20 db/decade or less represents a passivate state or general corrosion. From Fig.10, a high slope frequency of more than -20 db/decade was observed for corrosion of X65 pipeline steel at low temperatures, thus indicating a local corrosion process, whilst values at 25℃ indicated that corrosion was occurring through a combination of uniform and local corrosion processes.

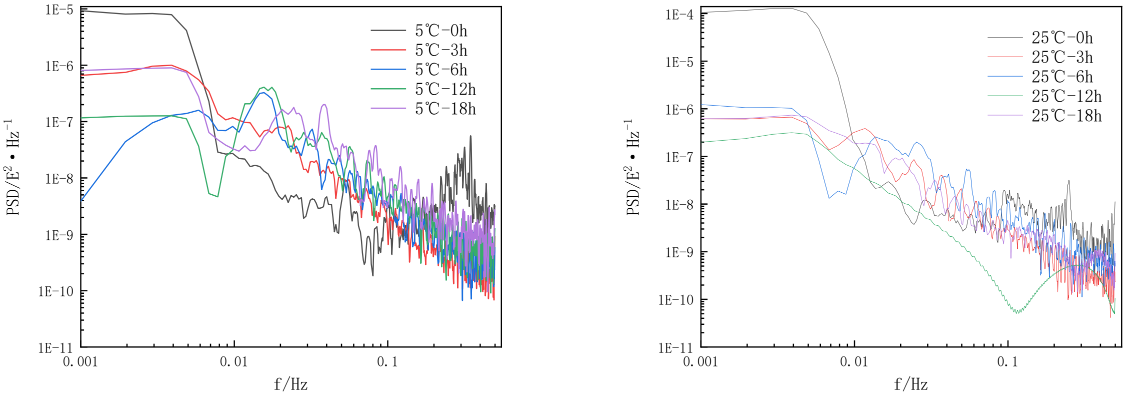

Figure 9. The PSD of potential noise of X65 steel with different immersion time at (a) 5℃ (b)25℃ (the black curve is 0 h, the red curve is 3 h, the blue curve is 6 h, the green curve is 12 h, the purple curve is 18 h)

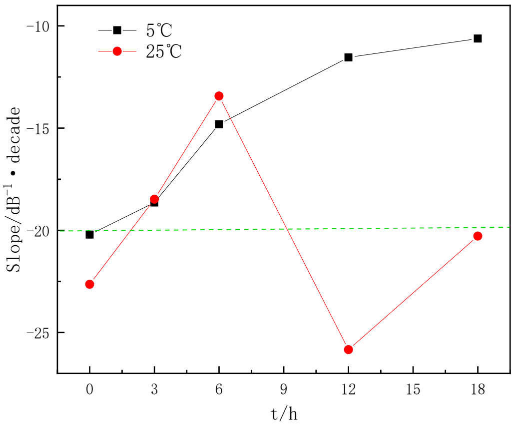

Figure 10. The roll off slopes of PSD of electrochemical noise at 5℃ and 25℃

3.4 Raman spectroscopy

The Raman spectrum of corrosion products after soaking in 3.5 % NaCl solution for 48 h at 5℃ and 25℃ was shown in Fig.11. The expected Raman peaks for iron oxide compounds in this experiment was listed in Table 4. At 5℃, Raman analysis revealed peaks at 274，366 and 1307 cm^{-1} that were assigned to γ-FeOOH, with peaks at 274 and 592 cm^{-1} assigned to Fe_3O_4. At 25℃, peaks located at 284 and 1304cm^{-1} were assigned to γ-FeOOH, with bands at 397, 485 and 588cm^{-1} assigned to α-FeOOH. Some studies [22] have reported that there are two reaction processes of γ-FeOOH, one is the reduction reaction and the product is the Fe_3O_4, which is the transformation between different valence states. The other is the product α-FeOOH, which is the transformation between different crystalline states of the same valence states. Therefore, the temperature changes reaction process of γ-FeOOH. As a cathode, the conductive Fe_3O_4 promotes the pitting of X65 steel at 5°C, which may be the cause of pitting at low temperatures.

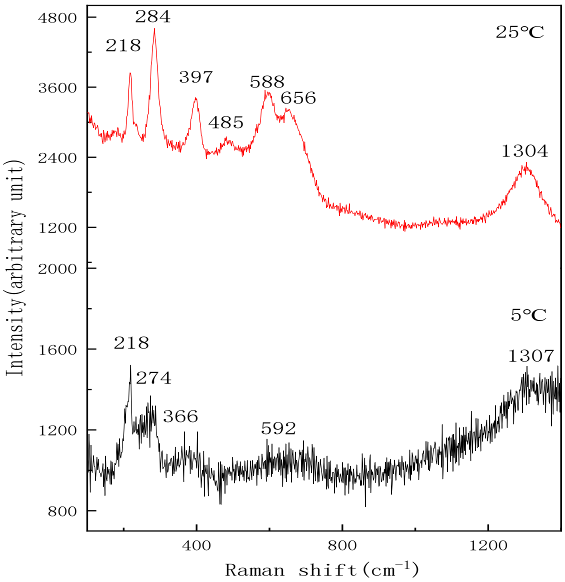

Figure 11. Raman spectrum of corrosion products of X65 steel after soaking for 48h at 5°C and 25°C

Table 4. The expected Raman peaks for iron oxide compounds

Compositions	Compounds	Raman shift (cm^{-1})	reference
α-FeOOH	Goethite	397,485,554	[23,24]
γ-FeOOH	Lepidocrocite	255,380,1307	[23,24]
FeO	Wustite	616,663	[24]
Fe_3O_4	Magnetite	297,540,616,663,680	[23,24,26]
α-Fe_2O_3	Hematite	295,415,500,615,1320	[24,26]
γ- Fe_2O_3	Maghemite	358,499,678,710	[25]

3.5 Corrosion morphology observation

The corrosion morphologies of X65 steel specimens at 5°C and 25°C under 15MPa hydrostatic press after soaking for 48 h were illustrated in Fig.12. As shown in Fig.12a, the corrosion product film was relatively uniform at 5°C. From Fig.12b the cracks on the corrosion product film was observed in 25°C environment, which indicated the presence of relatively porous α-FeOOH films. These results were consistent with the results of electrochemical impedance spectroscopy and Raman spectroscopy.

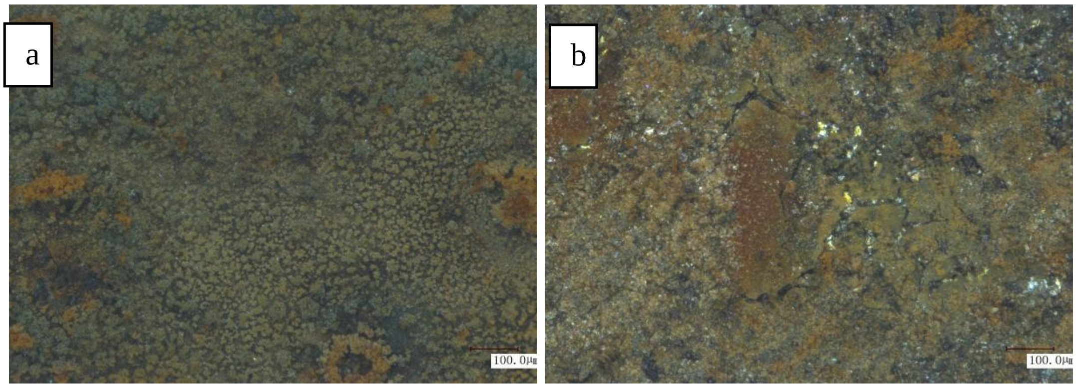

Figure 12. Morphologies of X65 steel corrosion productions after soaking for 48h at 5°C(a) and 25°C(b)

Removal of corrosion products enabled the surface of the X65 steel to be observed by 3D microscopy. As shown in Fig.13a, the corrosion of specimens featured pitting corrosion in 5°C environment and the surface filled with the uniform pits. The magnification morphology of the pits were similar to that in Fig.13d. It may be that the corrosion rates are relatively low at lower temperatures and the corrosion pits are not combined to form uniform corrosion. Conversely, images of samples kept at 25°C revealed uniform corrosion pattern (see Fig.13c), which was in accordance with the results obtained from electrochemical noise measurements.

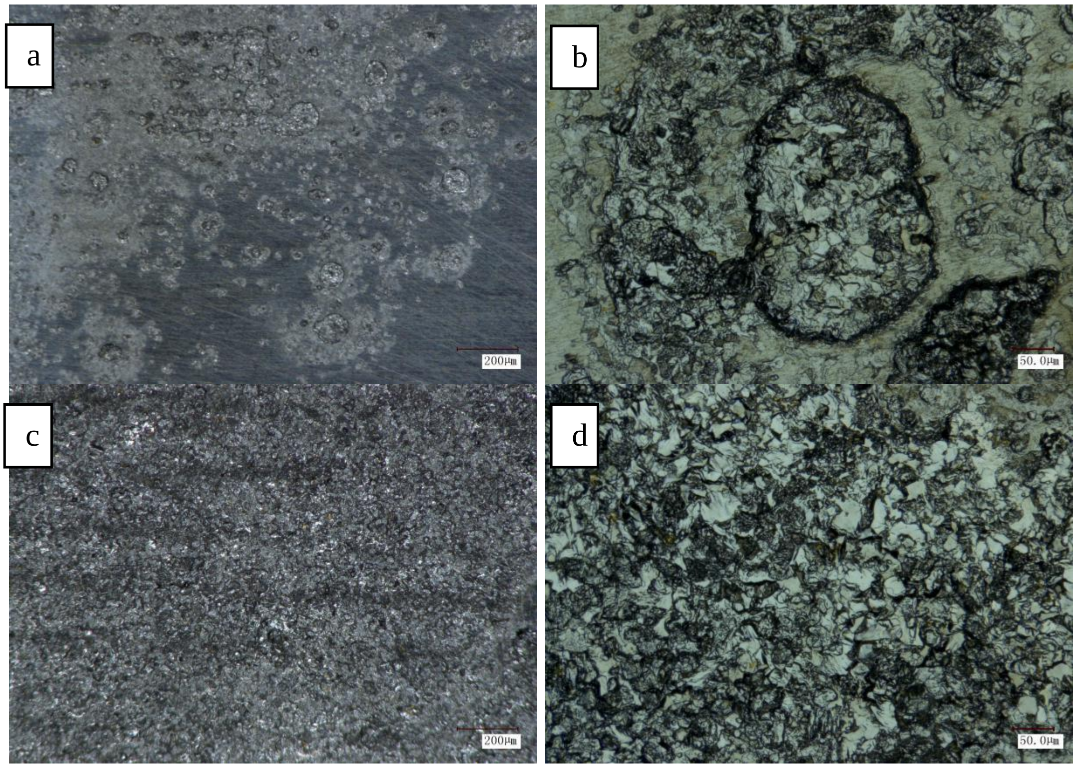

Figure 13. Morphologies of X65 steel corrosion productions after soaking for 48h at 5°C(a,b) and 25°C(c,d)

4. CONCLUSIONS

The influence of temperature on the corrosion behavior of X65 steel under 15MPa pressure has been investigated using electrochemical methods, Raman spectroscopy and 3D microscopy, with the aim to simulating the corrosion behavior of X65 steel in abyssal environments. The conclusions are summarized as below:

(1) The corrosion activity and kinetics of the corrosion reaction increases with the elevated temperature. The corrosion process is mainly controlled by the anodic reaction from 5℃ to 35℃, while that is primarily controlled by cathodic process at -5℃.

(2) The type of corrosion produced in X65 pipeline steel changed from a localized pitted corrosion process at low temperatures to a more uniform corrosion process as the temperature increased to 25℃.

(3) The temperature changes reaction process of γ-FeOOH. γ-FeOOH and Fe_3O_4 were formed as corrosion products at 5℃, while γ-FeOOH and α-FeOOH were produced at 25℃.

ACKNOWLEDGEMENTS
This project was supported by Major State Basic Research Program of China ("973"Program, No. 2014CB046805) and Nature Science Foundation of China (General Program No 51671144, 51371124) and Natural Science Foundation of Tianjin (No. 17JCTPJC47100). This work was supported by Supporting Plan Project of Tianjin City (16YFZCGX00100).

References

1. R. Venkatesan, M.A. Venkatasamy, T.A. Bhaskaran, E.S. Dwarakadasa, M. Ravindran, *Br. Corros. J.*, 37 (2002) 257.
2. T. Pierluigi, C. Elisa, *Ocean Eng*, 87 (2014) 10.
3. *R.E.* Melchers, *Corrosion*, 59 (2003) 319.
4. Z.X. Yang, B. Kan, J.X, *Int. J. Hydrogen Energy*, 42 (2017) 27446.
5. Y.G. Yang, T. Zhang, Y.W. Shao, G.Z. Meng, F.H. Wang, *Corros. Sci.*, 52 (2010) 2697.
6. Y.G. Yang, T. Zhang, Y.W. Shao, G.Z. Meng, F.H. Wang, *Corros. Sci.*, 73 (2013) 250.
7. T. Zhang, Y.G. Yang, Y.W. Shao, G.Z. Meng, F.H. Wang, *Electrochim. Acta*, 54 (2009) 3915.
8. F.L. Sun, S. Ren, Z. Li, Z.Y. Liu, X.G. Li, C.W. Du, *Mater. Sci. Eng., A*, 685 (2017) 145.
9. C.G. Soares, Y. Garbatov, A. Zayed, *Corros. Eng., Sci. Technol.*, 46 (2011) 524.
10. X.M. Yu, Y.L. Huang, W.J. Qu, A.P. Yadav, R.D. Marco, *Int. J. Electrochem. Sci.*, 9 (2014) 3760.
11. W. Yuan, F. Huang, J. Liu, Q. Hu, Y.F. Cheng, *Corros. Eng., Sci. Technol.*, (2018).
12. H.M. Shalaby, A.A. Hasan, F.A. Sabti, *Corros. Sci.*, 34 (1999) 292.
13. R.E. Melchers, *Corrosion*, 58 (2002) 768.
14. H.M. Ezuber, *Anti-Corros. Method. M.*, 56 (2009) 168.
15. S.L. Djeghaba, A. Benchettara, F. Kellou, V. Ji, *Arab. J. Sci. Eng.*, 39 (2014) 113.
16. R. Nevshupa, I. Martinez, S. Ramos, A. Arredondo, *Mar. Struct.*, 60 (2018) 226.
17. F. L. Laque, Marine corrosion; causes and prevention, *Coatings*, (1975) New York.
18. N. J. Laycock, *Corrosion*, 55 (1999) 590
19. C.Y. Chi, N. Li, J.J Xue, X.B. Li, L.K. Xu, *Corros. Prot.*, 30 (2009) 772.
20. J. C. Uruchurtu, J. L. Dawson, *Corrosion*, 43 (1987) 19.
21. J.B. Shi, J.H. Wang, K. Wang, D.H. Xia, *Electrochemistry*, 82 (2014) 647.

22. Y. Zou, Y. Zheng, Y. Wang, J. Wang, *Acta Metall Sin.*, 46 (2010) 123.
23. J. Dünnwald, A. Otto, *Corros. Sci.*, 29 (1989) 1167.
24. R.J. Thibeau, C.W. Brown, R.H. Heidersbach, *Appl. Spectrosc.*, 32 (1978) 532.
25. M. Hanesch, *Geophys. J. Int.*, 177 (2009) 941.
26. O.N. Shebanova, P. Lazor, *J. Raman Spectrosc.*, 34 (2003) 845.